International Journal of Heat and Mass Transfer 136 (2019) 99–115

Contents lists available at ScienceDirect

International Journal of Heat and Mass Transfer

journal homepage: www.elsevier.com/locate/ijhmt

Heat and mass transfer on rectangular and annular finned surfaces of heat exchangers operating under frosting conditions

Teresa Benítez [a], S.A. Sherif [a], J. Benítez [b,*]

[a] Department of Mechanical and Aerospace Engineering, University of Florida, P.O. Box 116300, Gainesville, FL 32611-6300, United States
[b] Department of Environmental Engineering Sciences, University of Florida, P.O. Box 116450, Gainesville, FL 32611-6450, United States

ARTICLE INFO

Article history:
Received 17 November 2018
Received in revised form 1 January 2019
Accepted 2 February 2019

Keywords:
Frost formation
Rectangular fin
Annular fin
Moving boundary
Orthogonal collocation
Heat transfer
Mass transfer
Super saturation

ABSTRACT

The analysis of the process of frost formation on a cold surface exposed to humid air yields a system of differential equations. In this study, the orthogonal collocation method is used to help solve the system of equations resulting from the flow of humid air over heat exchanger fins maintained at a temperature below both the dew-point temperature of water vapor in air and the freezing point. The temporal dependence of the frost growth creates a moving boundary that is addressed using a front-fixing method. This proposed method allows solving for important variables such as frost thickness, temperature distribution, and heat flux through the frost layer. Model results were found to agree closely with available experimental data. In all data sets modeled, it was found that super saturation at the frost-air interface must be included in the model to accurately predict frost growth.

1. Introduction

Frost formation on cold surfaces in heat exchanger and refrigeration applications has considerable practical relevance. The frost layer acts as a thermal insulator between the cooling surface and the air, decreasing the efficiency of the cooling process. It also reduces the size of the air channels, therefore increasing the generated pressure drop This was reported by many researchers such as Emery and Siegel [11] who found a 50–75% decrease in heat transfer and a substantial increase in pressure drop on the surface of a compact heat exchanger. Results obtained by Chen et al. [6] and Su [31] show a comparable trend. Therefore, an accurate and robust analysis of the frost formation process is essential to characterize the aforementioned problems.

Analyzing the structure and properties of a frost layer is challenging to do. The frost formation process is three-dimensional, non-linear, transient, and involves coupled heat and mass transfer with a moving boundary. The structure within the frost varies continuously [21], and as recently as 2015, a detailed physical description of the unsteady frost formation process was not clear [19]. In terms of experimental data acquired, it is also difficult to investigate, due to the unstable and brittle nature of the deposited frost [24].

Chen et al. [5,6] studied frost formation on rectangular fins, experimentally and analytically. They developed a test facility to characterize frost growth on heat exchanger fins where the cold surfaces and the air supply conditions were similar to those experienced in freezers. This facility included a test section with removable fins to measure the frost height and mass concentration. They presented results for typical operating conditions with frost growth on fins. They presented data for frost height on fins, increase in pressure loss, frost mass accumulation, and heat transfer rate. Kim et al. [20] proposed a mathematical model for predicting frost behavior on a heat exchanger fin under frosting conditions, considering fin heat conduction. Their model reflected the change in the three-dimensional airside flow caused by frost growth. Kim et al. [18] conducted frosting experiments to analyze the characteristics of frost formation on a two-dimensional fin with a non-uniform temperature distribution. The temperature distribution and the characteristics of frost formation were analyzed perpendicular and parallel to the airflow for different values of fin thickness and other frosting parameters.

Lenic et al. [25] developed a PDE-based model to describe transient two-dimensional frost formation on a fin-and-tube heat exchanger. The governing equations were discretized using the control volume method. The convection-diffusion terms were

* Corresponding author.
E-mail addresses: teresa.benitez@upr.edu (T. Benítez), sasherif@ufl.edu (S.A. Sherif), jaime.benitez@ufl.edu (J. Benítez).

https://doi.org/10.1016/j.ijheatmasstransfer.2019.02.005
0017-9310/

Nomenclature

A	first-derivative matrix for orthogonal collocation, dimensionless
B	second-derivative matrix for orthogonal collocation, dimensionless
B_c	proportion of frost volume representing ice spheres and ice planes
C	specific heat at constant pressure, kJ kg^{-1} K^{-1}
d	fins half-thickness, m
D_{AB}	molecular diffusivity of water vapor in air, m^2 s^{-1}
D_{eff}	effective mass diffusivity of water vapor inside the frost, m^2 s^{-1}
D_K	water vapor Knudsen diffusivity inside frost, m^2 s^{-1}
f	friction factor, dimensionless
h	convective heat-transfer coefficient, W m^{-2} K^{-1}
h_m	convective mass-transfer coefficient, m s^{-1}
h_{sg}	latent heat of sublimation of ice, kJ kg^{-1}
j_D	Colburn j-factor for mass transfer, dimensionless
j_H	Colburn j-factor for heat transfer, dimensionless
k	thermal conductivity, W m^{-1} K^{-1}
k_{eff}	effective thermal conductivity of frost, W m^{-1} K^{-1}
k_l	lower limit of thermal conductivity
k_u	upper limit of thermal conductivity
L	fin length, m
$\dot{m}$	volumetric rate of ice deposition, kg m^{-3} s^{-1}
N	number of interior collocation points
Nu_D	Nusselt number based on hydraulic diameter, dimensionless
Pr	Prandtl number, dimensionless
Q	dimensionless heat flux through cold surface
q_{f0}	volumetric heat flow rate, W m^{-3}
r	radial coordinate, m
Re_D	Reynolds number based on hydraulic diameter, dimensionless
S	degree of super saturation, dimensionless
T	absolute temperature, K
t	time, s
t_{fin}	fins spacing, m
V	gas velocity, m s^{-1}
w	quadrature weight, dimensionless
x	coordinate axis, m
z	coordinate axis, m

Greek symbols

α_t	absorption factor, dimensionless
δ_f	frost thickness, m
ε	volumetric fraction
γ	dimensionless radial coordinate
η	dimensionless coordinate axis
ρ	mass density, kg m^{-3}
ξ	dimensionless coordinate axis
τ	tortuosity, dimensionless
θ	dimensionless temperature for rectangular fin [Eq. (37)]
Θ	dimensionless temperature for annular fin [Eq. (77)]
θ_c	parameter in Dietenberger [9] model

Subscripts

a	dry air
b	base wall
F	fin
f	frost
s	frost surface
sat	saturation
v	water vapor
β	ice phase
0	initial
∞	ambient

treated using a power-law scheme. An iterative procedure was used to solve the resulting set of linearized discretization equations. Lee et al. [23] provided experimental data to be used to predict frost growth and frost performance of a round plate fin-tube heat exchanger for low temperature heat pumps used in zero emission vehicles under cold weather conditions. Round plate fin-tube heat exchangers were tested with variation of the fin space, airflow rate, relative humidity, and inlet air temperature. Frost height was measured. The variation of the blockage ratio with fin space was determined to be an important parameter when designing advanced heat exchangers that operate in cold weather conditions.

Mahdavi and Yaghoubi [27] experimentally measured the natural convection heat transfer and frost deposition over a horizontal fin-tube. The fins were annular, with a small fin pitch (2 mm), common in air-cooled heat exchangers and some refrigerated evaporators. Hirbodi and Yaghoubi [14] experimentally investigated heat and mass transfer during natural condensation of humid air over a horizontal annular finned-tube. The fins were circular with rectangular cross-section. The test results showed that condensation and heat transfer rate depend mainly on the temperature and relative humidity of the surrounding air and fin base temperature. Correlations were developed for heat and mass transfer during natural dehumidification over compact annular finned-tubes. Their correlations, expressed in terms of the Rayleigh number, were based on those of Chen and Hsu [7] modified by Mahdavi and Yaghoubi [27].

This paper uses a methodology, first suggested by Benítez and Sherif [3] with regards to frost formation on a flat plate, to approximate the solution to the system of PDEs that describe the frost formation process on heat exchanger fins. First, the front-fixing method [8] is used to determine a suitable set of new coordinates that deal with the moving boundary. Then, with the orthogonal collocation method [1,4,10,29,33] the transformed system of differential equations is converted to an initial value problem. The solution to this problem is carried out using an ODE solver from MATLAB. The results obtained from the model are compared to available data in the literature.

While the previous work by Benítez and Sherif [3] was limited to the simple one-dimensional geometry of a flat plate with uniform wall temperature, this paper extends the analysis to more complex geometries such as rectangular and annular fins. In these applications, heat and mass transfer considerations are by nature two-dimensional, adding a significant level of complexity to the problem. From the point of view of practical application of the results, analysis of rectangular and annular fins is much more attractive due to their widespread use in refrigeration applications where frost formation is a very important drawback.

Analysis of the dynamics of frost formation over extended surfaces have gone from the simple quasi steady-state approximation [26] to the use of sophisticated computational fluid dynamics (CFD) models using grid sizes of over 100,000 points [19]. The methodology presented in this paper fills the gap between those

extremes. The solution of the resulting set of algebraic equations can be easily programmed in MATLAB, a widely available computing platform.

The use of orthogonal collocation has several distinctive advantages. Because of the special mathematical properties of orthogonal polynomials, discretization of the PDEs using the prescribed collocation points allows the researcher to use a much smaller number of grid points while obtaining very accurate results [10]. Besides, the solutions obtained at the collocation points can be easily used to accurately estimate both space derivatives and integrals of the dependent variables. Those are important tools for heat- and mass-transfer calculations of fluxes and average frost properties.

2. General analysis

The frost layer is treated as a porous medium with a distributed porosity and expanding boundary. The volume averaging technique [34] is used to formulate the problem. The frost layer consists of a β-phase (solid ice) surrounded by a γ-phase (water vapor and air). The major assumptions used to develop the governing equations with their corresponding boundary conditions are: (a) heat and mass transport within the frost layer occur in two directions perpendicular to each other; (b) heat transport in the fin is assumed to be only in one direction; (c) the total pressure of the gaseous phase in the frost is constant; (d) the temperatures of the gaseous and solid phases inside the frost layer are the same; (e) convection of the gaseous phase within the frost is negligible compared to molecular diffusion inside the pores of the frost layer; (f) the amount of water vapor that deposits as ice within the frost is proportional to the water vapor density in the pores of the frost layer; (g) the gradient of the ice volume fraction at the boundaries of the frost layer is equal to zero; (h) the frost thickness does not vary along the length of the fin; (i) the temperature and humidity of the air are assumed constant with respect to time; and (j) the physical properties of the fin are constant.

Assumption (a) differs significantly from that in the previous work by Benítez and Sherif [3], in which frost formation on a flat plate was modeled. This assumption substantially alters the mathematical formulation of the model, as is shown in this section where separate sets of governing equations—with accompanying boundary and initial conditions—are developed for the fin and for the frost.

2.1. Governing equations

For a spatial domain consisting of the entire length of the fin, the temperature distribution of the fin, T_F, can be described by the following energy equation (assuming that the properties of the fin are constant):

Energy equation (fin)

$$C_F \rho_F \frac{\partial T_F}{\partial t} = k_F \nabla^2 T_F + q_{f0} \tag{1}$$

In this equation, T_F is the fin temperature distribution and q_{f0} is the volumetric heat flow rate by conduction normal to the fin-frost interface. (The symbols are listed in the Nomenclature.)

For a spatial domain consisting of the total thickness of the frost layer, the temperature distribution for the frost, T_f, volume fraction of the ice phase, ε_β, and the vapor phase density, ρ_v, can be described by the following governing equations:

Energy equation (frost)

$$C_f \rho_f \frac{\partial T_f}{\partial t} = \nabla \cdot (k_{eff} \nabla T_f) + \dot{m} h_{sg} \tag{2}$$

Continuity equation for ice in the frost

$$\frac{\partial \varepsilon_\beta}{\partial t} = \frac{\dot{m}}{\rho_\beta} \tag{3}$$

Continuity equation for water vapor in the gas phase

$$\frac{\partial}{\partial t}\left[\rho_v (1-\varepsilon_\beta)\right] = \nabla \cdot (D_{eff} \nabla \rho_v) - \dot{m} \tag{4}$$

Later in this article, Eqs. (1)–(4) will be written for two distinct geometries: rectangular and annular fins. At that time, the required initial and boundary conditions will be specified.

2.2. Physical properties of the frost

The properties of the frost in Eqs. (2) and (4) depend on local conditions of the frost, such as temperature and ice volume fraction. Correlations to estimate those properties are given next.

2.2.1. Frost density

The density of the frost is a function of the density of the ice, the density of the air, and the density of the water vapor. The density of the ice is much greater than the density of the mixture of gases. Therefore, the density of the frost is approximately

$$\rho_f = \varepsilon_\beta \rho_\beta + (1-\varepsilon_\beta)(\rho_a + \rho_v) \approx \varepsilon_\beta \rho_\beta \tag{5}$$

2.2.2. Frost specific heat

A similar reasoning can be used for the approximation of the specific heat of the frost

$$C_f = \frac{\varepsilon_\beta \rho_\beta C_\beta + (1-\varepsilon_\beta)(C_a \rho_a + C_v \rho_v)}{\rho_f} \approx \frac{\varepsilon_\beta \rho_\beta C_\beta}{\rho_f} \approx C_\beta \tag{6}$$

2.2.3. Frost thermal conductivity

$$k_{eff} = \frac{1}{4}\Big[(3B_c - 1)k_l + (3\theta_c - 1)k_u + \Big(\{(3B_c - 1)k_l + (3\theta_c - 1)k_l\}^2 + 8k_l k_u\Big)^{1/2}\Big] \tag{7}$$

Eq. (7) was developed by Dietenberger [9] to estimate the effective thermal conductivity of the frost as a function of temperature and ice volume fraction. The model uses the following assumptions about the frost structure: (1) at low frost density or at high porosity, two types of frost structure predominate. One is formed of ice cylinders created by the diffusion of water vapor or water droplets; (2) the resulting conductive heat transfer is much higher in the ice cylinders than in the spheres; and (3) at high frost densities or low porosities, the total frost structure is a random mixture of air bubbles and ice layers, with enhanced thermal conduction. Using known expressions for the conductivities of ice cylinders, ice spheres, ice planes and air bubbles, expressions for the four parameters of the model (k_l, k_u, B_c, and θ_c) were derived in terms of frost temperature and ice volume fraction.

2.2.4. Effective mass diffusivity

The expression for the effective mass diffusivity inside the frost combines the mechanisms of Knudsen and molecular diffusion characteristic of diffusion inside porous media [30],

$$D_{eff} = \frac{1-\varepsilon_\beta}{\tau}\left(\frac{D_{AB}}{1 + D_{AB}/D_K}\right) \tag{8}$$

Here, D_{AB} is the molecular diffusivity of water vapor in air, D_K is the Knudsen diffusivity of water vapor inside the pores, and τ is the tortuosity of the pores. The Knudsen diffusivity depends on the characteristic pore diameter, a parameter not known for frost. The

tortuosity can be estimated in terms of the frost porosity, according to Na and Webb [28]. The following expression is obtained

$$D_{eff} = \frac{(1-\varepsilon_\beta)(2-\varepsilon_\beta)}{2}\left(\frac{D_{AB}}{1+D_{AB}/D_K}\right) \tag{9}$$

The ratio D_{AB}/D_K is approximately 8.0, a value typical of porous media [2,3] The value of D_{AB} was calculated as suggested by Mago and Sherif [26].

3. Analysis of rectangular fin

Fig. 1 is a schematic diagram of a rectangular fin with a frost layer of thickness $\delta_f(t)$ growing on both sides of the extended surface.

3.1. Governing equations

For rectangular geometry, Eqs. (1), (2), and (4) can be written as (assuming heat transfer only in the x direction for the fin, and in the x and z directions for the frost layer):

$$\frac{\partial T_F}{\partial t} = \frac{k_{eff}}{\rho_F C_F d}\frac{\partial T_f}{\partial z}\bigg|_{z=0} + \frac{k_F}{C_F\rho_F}\frac{\partial^2 T_F}{\partial x^2} \tag{10}$$

$$\frac{\partial T_f}{\partial t} = \frac{\dot{m}h_{sg}}{\rho_f C_f} + \frac{1}{\rho_f C_f}\left[k_{eff}\frac{\partial^2 T_f}{\partial z^2} + \frac{\partial T_f}{\partial z}\frac{\partial k_{eff}}{\partial z} + k_{eff}\frac{\partial^2 T_f}{\partial x^2} + \frac{\partial T_f}{\partial x}\frac{\partial k_{eff}}{\partial x}\right] \tag{11}$$

$$\frac{\partial}{\partial t}\left[\rho_v(1-\varepsilon_\beta)\right] = D_{eff}\frac{\partial^2\rho_v}{\partial z^2} + \frac{\partial\rho_v}{\partial z}\frac{\partial D_{eff}}{\partial z} + D_{eff}\frac{\partial^2\rho_v}{\partial x^2} + \frac{\partial\rho_v}{\partial x}\frac{\partial D_{eff}}{\partial x} - \dot{m} \tag{12}$$

3.2. Initial conditions

Assuming that the temperature profile in the fin reaches steady state before frost formation begins, we have [15],

$$T_F(x,t=0) = T_\infty - (T_b - T_\infty)\frac{\cosh[m_F(L-x)]}{\cosh(m_F L)} \qquad m_F^2 = \frac{h}{k_F d} \tag{13}$$

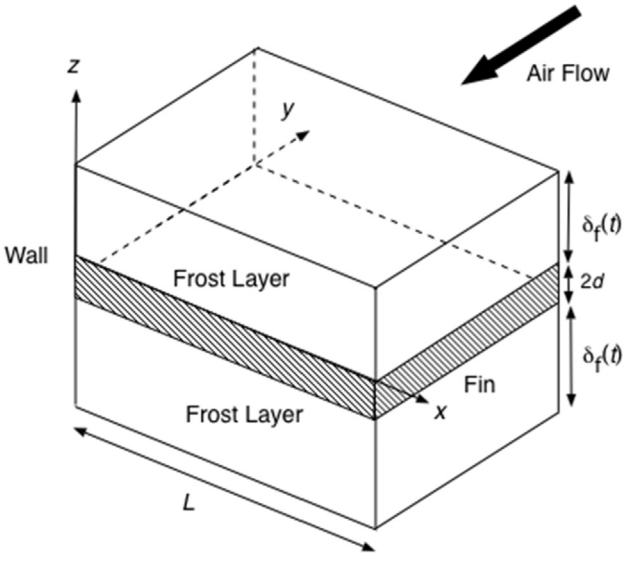

Fig. 1. Rectangular fin covered by a uniform frost layer.

$$T_f(x,z,t=0) = T_F(x,t=0) \tag{14}$$

$$\delta_f(t=0) = \delta_0 \tag{15}$$

$$\varepsilon_\beta(t=0) = \varepsilon_{\beta 0} \tag{16}$$

$$\rho_v(x,z,t=0) = \rho_{v_{sat}}(T_F) \tag{17}$$

In Eq. (14), it is assumed that the initial frost layer is in thermal equilibrium with the fin. The initial values for frost layer thickness and density, shown in Eqs. (15) and (16), were investigated by Jones and Parker [16] who determined that these values were around 0.02 mm and 30 kg/m^3, respectively. In Eq. (17), it is assumed that the gas phase in the initial frost layer is saturated with water vapor at the local temperature.

3.3. Boundary conditions

For the fin we can write

$$T_F|_{x=0} = T_b \tag{18}$$

$$\frac{\partial T_F}{\partial x}\bigg|_{x=L} = 0 \tag{19}$$

At the interface between the fin and the frost layer we have

$$T_f|_{x,z=0} = T_F(x) \tag{20}$$

$$\frac{\partial\varepsilon_\beta}{\partial z}\bigg|_{x,z=0} = 0 \tag{21}$$

$$\frac{\partial\rho_v}{\partial z}\bigg|_{x,z=0} = 0 \tag{22}$$

At the interface between the frost layer and the air we have

$$k_{eff}\frac{\partial T_f}{\partial x}\bigg|_{x,z=\delta_f} = h\left(T_\infty - T_f|_{x,z=\delta_f}\right) + h_{sg}\rho_f\big|_{x,z=\delta_f}\frac{d\delta_f}{dt} \tag{23}$$

$$\frac{\partial\varepsilon_\beta}{\partial z}|_{x,z=\delta_f} = 0 \tag{24}$$

$$D_{eff,s}\overline{\frac{\partial\rho_v}{\partial z}}\bigg]_{z=\delta_f} + \rho_f\big]_{z=\delta_f}\frac{d\delta_f}{dt} = h_m\left(\rho_{v,\infty} - \overline{\rho_v}\right]_{x,z=\delta_f}\Big) \tag{25}$$

$$\rho_v|_{x,z=\delta_f} = (1+S)\rho_{v_{sat}}\left(T_f|_{x,z=\delta_f}\right) \tag{26}$$

Eq. (23) is an energy balance at the interface and states the fact that the energy transferred to the frost layer from the humid air by convection, plus the latent energy released when the water vapor deposits as ice on the surface, move toward the inside of the frost layer by conduction. Eq. (25) is a water vapor mass balance at the interface. Part of the water vapor transferred from the humid air to the frost layer by convection diffuses into the layer contributing to its densification, while the rest deposits as ice on the surface, thus increasing the frost layer thickness. Therefore, the boundary between the frost layer and the air will be moving as the frost layer thickness increases.

Eq. (26) introduces the possibility of super saturation at the interface between frost and air. Most researchers assume that the water vapor density at the interface corresponds to saturation conditions at the frost surface temperature. If that were the case, once the surface temperature is calculated, the corresponding water vapor density would be fixed. However, Na and Webb [28] demonstrated that a certain degree of super saturation at the solid-vapor interface is required for ice crystal growth.

The required degree of super saturation is strongly dependent on the surface energy, the relative humidity of the air, and the temperature of the solid-vapor interface [17]. Na and Webb [28] developed a semi-empirical equation to predict the required degree of super saturation for a very restricted set of experimental conditions, based on a boundary-layer theory analysis. As far as we know, there is no general method for predicting the degree of super-saturation and it must be estimated by fitting an appropriate mathematical model (including it as an adjustable parameter) to experimental data.

At the fin base ($x = 0$), for the frost layer, we have

$$T_f\big|_{x=0,z} = T_b \tag{27}$$

$$\left.\frac{\partial \varepsilon_\beta}{\partial z}\right|_{x=0,z} = 0 \tag{28}$$

$$\left.\frac{\partial \rho_v}{\partial x}\right|_{x=0,z} = 0 \tag{29}$$

At the fin tip ($x = L$), for the frost layer, we have

$$\left.\frac{\partial T_f}{\partial x}\right|_{x=L,z} = 0 \tag{30}$$

$$\left.\frac{\partial \varepsilon_\beta}{\partial x}\right|_{x=L,z} = 0 \tag{31}$$

$$\rho_v\big|_{x=L,z} = (1+S)\rho_{v_{sat}}\left(T_f\big|_{x=L,z}\right) \tag{32}$$

3.4. Dimensionless coordinates and front-fixing method

A moving boundary can be fixed by the front-fixing method defining a new space coordinate [8]. Define the new dimensionless coordinates as:

$$\eta = \frac{z}{\delta_f(t)} \quad \xi = \frac{x}{L} \tag{33}$$

Assuming that the average frost thickness is independent of position, the first part of Eq. (33) fixes the frost moving boundary at a value of $\eta = 1$ for all t. By using the following relationships, the governing equations and boundary conditions can be expressed in terms of the dimensionless coordinates.

$$\frac{\partial}{\partial z} = \frac{1}{\delta_f}\frac{\partial}{\partial \eta} \quad \frac{\partial^2}{\partial z^2} = \frac{1}{\delta_f^2}\frac{\partial^2}{\partial \eta^2} \tag{34}$$

$$\frac{\partial}{\partial x} = \frac{1}{L}\frac{\partial}{\partial \xi} \quad \frac{\partial^2}{\partial x^2} = \frac{1}{L^2}\frac{\partial^2}{\partial \xi^2} \tag{35}$$

$$\left.\frac{\partial}{\partial t}\right|_{x,z} = \left.\frac{\partial}{\partial t}\right|_{\xi,\eta} - \frac{\eta}{\delta_f}\frac{d\delta_f}{dt}\frac{\partial}{\partial \eta} \tag{36}$$

It is convenient at this point to define dimensionless temperatures, θ, such that

$$\theta_f(t,\xi,\eta) = \frac{T_f(t,\xi,\eta) - T_b}{T_\infty - T_b} \quad \theta_F(t,\xi) = \frac{T_F(t,\xi) - T_b}{T_\infty - T_b} \tag{37}$$

3.5. Rate of ice deposition

The rate of ice deposition can be expressed as proportional to the water vapor density in the frost layer, as mentioned in assumption (f). For the pseudo-steady-state case, Lee et al. [21] found that

$$\dot{m} = \alpha_t \frac{D_{eff}}{\delta_f^2}\rho_v \tag{38}$$

The parameter α_t is given by [21], modified here to include super saturation,

$$\alpha_t = \left[\cosh^{-1}\left\{\frac{(1+S)\rho_{v_{sat}}(T_{f,s})}{\rho_{v_{sat}}(T_b)}\right\}\right]^2 \tag{39}$$

3.6. Modified governing equations

Applying the above, the governing equations become as follows:

3.6.1. Energy equation on the fin

Eq. (10) is written in terms of the dimensionless variables θ_F, ξ and η. The resulting energy equation of the fin is

$$\frac{\partial \theta_F}{\partial t} = \frac{k_{eff}\big|_{\eta=0}}{\delta_f \rho_F C_F d}\left.\frac{\partial \theta_f}{\partial \eta}\right|_{\eta=0} + \frac{k_F}{C_F \rho_F L^2}\frac{\partial^2 \theta_F}{\partial \xi^2} \tag{40}$$

3.6.2. Conservation of energy equation in the frost

Eq. (11) is written in terms of the dimensionless variables θ_f, ξ, and η and the volumetric rate of ice deposition, $\dot{m}$, to give

$$\begin{aligned}\frac{\partial \theta_f}{\partial t} = {} & \frac{\eta}{\delta_f}\frac{d\delta_f}{dt}\frac{\partial \theta_f}{\partial \eta} + \frac{\alpha_t D_{eff}\rho_v h_{sg}}{\rho_f C_f \delta_f^2 (T_\infty - T_b)} + \frac{k_{eff}}{\rho_f C_f \delta_f^2}\frac{\partial^2 \theta_f}{\partial \eta^2} \\ & + \frac{1}{\rho_f C_f \delta_f^2}\frac{\partial \theta_f}{\partial \eta}\frac{\partial k_{eff}}{\partial \eta} + \frac{k_{eff}}{\rho_f C_f L^2}\frac{\partial^2 \theta_f}{\partial \xi^2} + \frac{1}{\rho_f C_f L^2}\frac{\partial \theta_f}{\partial \xi}\frac{\partial k_{eff}}{\partial \xi}\end{aligned} \tag{41}$$

3.6.3. Continuity equation for ice in the frost

$$\frac{\partial \varepsilon_\beta}{\partial t} = \frac{\alpha_t D_{eff}\rho_v}{\delta_f^2 \rho_\beta} + \frac{\eta}{\delta_f}\frac{d\delta_f}{dt}\frac{\delta \varepsilon_\beta}{\delta \eta} \tag{42}$$

3.6.4. Continuity equation for water vapor in the air

Eq. (12) is the continuity equation for water vapor in the air. First, it is written in terms of the dimensionless variables. Then, the volumetric rate of ice deposition expression is inserted. The continuity equation becomes

$$\begin{aligned}\frac{\partial \rho_v}{\partial t} = {} & \frac{\rho_v}{(1-\varepsilon_\beta)}\frac{\partial \varepsilon_\beta}{\partial t} + \frac{\eta}{\delta_f}\frac{d\delta_f}{dt}\frac{\partial \rho_v}{\partial \eta} - \frac{\eta \rho_v}{\delta_f(1-\varepsilon_\beta)}\frac{d\delta_f}{dt}\frac{\partial \varepsilon_\beta}{\partial \eta} - \frac{\alpha_t D_{eff}\rho_v}{\delta_f^2(1-\varepsilon_\beta)} \\ & + \frac{D_{eff}}{\delta_f^2(1-\varepsilon_\beta)}\frac{\partial^2 \rho_v}{\partial \eta^2} + \frac{1}{\delta_f^2(1-\varepsilon_\beta)}\frac{\partial \rho_v}{\partial \eta}\frac{\partial D_{eff}}{\partial \eta} \\ & + \frac{D_{eff}}{(1-\varepsilon_\beta)L^2}\frac{\partial^2 \rho_v}{\partial \xi^2} + \frac{1}{(1-\varepsilon_\beta)L^2}\frac{\partial \rho_v}{\partial \xi}\frac{\partial D_{eff}}{\partial \xi}\end{aligned} \tag{43}$$

The rate of increase of the frost layer thickness is obtained from Eq. (25), written in terms of the dimensionless variables:

$$\frac{d\delta_f}{dt} = \frac{h_m\left(\rho_{v,\infty} - \overline{\rho_v}\big|_{\eta=1}\right)}{\rho_f\big|_{\eta=1}} - \frac{D_{eff,s}}{\delta_f \rho_f\big|_{\eta=1}}\left.\frac{\overline{\partial \rho_v}}{\partial \eta}\right|_{\eta=1} \tag{44}$$

Eqs. (40)–(44) form a set of nonlinear, coupled PDEs whose solution must be obtained by a suitable numerical method.

3.7. Orthogonal collocation method

The method developed by Villadsen and Stewart [32,33] is one of a general class of approximate methods for boundary value problems known as the Method of Weighted Residuals [29]. The spatial dimensions are discretized using N internal collocation points. With rectangular geometry and no symmetry, both boundaries are included as additional collocation points for a total of $N+2$ discretization points for each dimension, chosen specifically as the roots of the $(N+2)$ degree Jacobi orthogonal polynomial [10]. Benítez and Sherif [3] effectively used this method to describe the frost formation process on flat plates.

The spatial derivatives are discretized as follows (illustrated here with the dimensionless temperature, but applicable to other properties)

$$\left.\frac{\partial\theta}{\partial\xi}\right|_{i,k}=\sum_{j=1}^{N+2}Ax(i,j)\theta(j,k)\quad\left.\frac{\partial^2\theta}{\partial\xi^2}\right|_{i,k}=\sum_{j=1}^{N+2}Bx(i,j)\theta(j,k)\tag{45}$$

$$\left.\frac{\partial\theta}{\partial\eta}\right|_{i,k}=\sum_{l=1}^{M+2}Az(k,l)\theta(i,l)\quad\left.\frac{\partial^2\theta}{\partial\eta^2}\right|_{i,k}=\sum_{l=1}^{M+2}Bz(k,l)\theta(i,l)\tag{46}$$

where $i=1,2,\cdots,M+2\quad k=1,2,\cdots,M+2$

Matrices **Ax, Az, Bx,** and **Bz** are readily calculated once the value of N, the geometry of the problem, and whether one or two of the boundaries are included as collocation points are specified [3]. Do [10] gives MATLAB programs to calculate the roots, and the matrices **Ax, Az, Bx,** and **Bz.** The results obtained through the orthogonal can be used directly to accurately estimate spatial integrals by means of a quadrature formula. This is very useful for estimating average properties of the frost layer, such as temperature, and density, as follows

$$\overline{\rho_f}(t)=\frac{1}{\delta_f}\int_0^{\delta_f}\rho_f(t,z)dz=\int_0^1\rho_f(t,\eta)d\eta\approx\sum_{j=1}^{N+2}w_j\rho_f\left(t,\eta_j\right)\tag{47}$$

In this equation, w_j is the quadrature weight corresponding to the root η_j. The weights are obtained from the MATLAB program given by Do [10].

The governing Eqs. (40)–(43) must be satisfied at each of the N internal collocation points. They become:

$$\frac{d\theta_F(i)}{dt}=\frac{k_{eff}|_{\eta=0}}{\delta_f\rho_FC_Fd}\sum_{l=1}^{N+2}Az(1,l)\theta_f(i,l)+\frac{k_F}{\rho_FC_FL^2}\sum_{j=1}^{N+2}Bx(i,j)\theta_F(j)\tag{48}$$

$$\begin{aligned}\frac{d\theta_f(i,k)}{dt}=&\frac{\eta_k}{\delta_f}\frac{d\delta_f}{dt}\sum_{l=1}^{M+2}Az(k,l)\theta_f(i,l)+\frac{\alpha_tD_{eff}(i,k)h_{sg}\rho_v(i,k)}{\delta_fC_f\delta_f^2(T_\infty-T_b)}\\&+\frac{1}{\delta_fC_f\delta_f^2}\left(\sum_{l=1}^{M+2}Az(k,l)\theta_f(i,l)\sum_{l=1}^{M+2}Az(k,l)k_{eff}(i,l)\right.\\&\left.+k_{eff}(i,k)\sum_{l=1}^{M+2}Bz(k,l)\theta_f(i,l)\right)\\&+\frac{1}{\delta_fC_fL^2}\left(\sum_{j=1}^{N+2}Ax(i,j)\theta_f(j,k)\sum_{j=1}^{N+2}Ax(i,j)k_{eff}(j,k)\right.\\&\left.+k_{eff}(i,k)\sum_{j=1}^{N+2}Bx(i,j)\theta_f(j,k)\right)\end{aligned}\tag{49}$$

$$\frac{d\varepsilon_\beta(i,k)}{dt}=\frac{\alpha_tD_{eff}(i,k)\rho_v(i,k)}{\delta_f^2\rho_\beta}+\frac{\eta_k}{\delta_f}\frac{d\delta_f}{dt}\sum_{l=1}^{M+2}Az(k,l)\varepsilon_\beta(i,l)\tag{50}$$

$$\begin{aligned}\frac{d\rho_v(i,k)}{dt}=&\frac{\rho_v(i,k)}{[1-\varepsilon_\beta(i,k)]}\frac{\partial\varepsilon_\beta(i,k)}{\partial t}+\frac{\eta_k}{\delta_f}\frac{d\delta_f}{dt}\sum_{l=1}^{M+2}Az(k,l)\rho_v(i,l)\\&-\frac{\eta_k\rho_v(i,k)}{\delta_f[1-\varepsilon_\beta(i,k)]}\frac{d\delta_f}{dt}\sum_{l=1}^{M+2}Az(k,l)\varepsilon_\beta(i,l)\\&-\frac{\alpha_tD_{eff}(i,k)\rho_v(i,k)}{\delta_f^2[1-\varepsilon_\beta(i,k)]}+\frac{1}{[1-\varepsilon_\beta(i,k)]\delta_f^2}\\&\times\left(\sum_{l=1}^{M+2}Az(k,l)\rho_v(i,l)\sum_{l=1}^{M+2}Az(k,l)D_{eff}(i,l)+D_{eff}(i,k)\sum_{l=1}^{M+2}Bz(k,l)\rho_v(i,l)\right)\\&+\frac{1}{[1-\varepsilon_\beta(i,k)]L^2}\\&\times\left(\sum_{j=1}^{N+2}Ax(i,j)\rho_v(j,k)\sum_{j=1}^{N+2}Ax(i,j)D_{eff}(j,k)+D_{eff}(i,k)\sum_{j=1}^{N+2}Bx(i,j)\rho_v(j,k)\right)\end{aligned}\tag{51}$$

Eq. (44) is written in terms of orthogonal collocation as:

$$\begin{aligned}\frac{d\delta_f}{dt}=&\frac{h_m\left(\rho_{v,\infty}\sum_{i=1}^{N+2}w_i\rho_v(i,N+2)\right)}{\rho_\beta\sum_{i=1}^{N+2}w_i\varepsilon_\beta(i,N+2)}\\&-\frac{D_{eff,s}}{\rho_\beta\delta_f\sum_{i=1}^{N+2}w_i\varepsilon_\beta(i,N+2)}\sum_{i=1}^{N+2}w_i\sum_{j=1}^{N+2}Az(N+2,j)\rho_v(i,N+2)\end{aligned}\tag{52}$$

In Eq. (52), the frost density at any point is approximated with the product of the ice density and the ice volume fraction, as justified above. The boundary conditions must also be expressed in terms of the collocation points.

Eqs. (48)–(52), with initial conditions given by Eqs. (13)–(17), constitute an initial value problem (IVP) that can be approximately solved using the ode15s program of MATLAB.

4. Analysis of annular fin

Fig. 2 is a schematic diagram of an annular fin with a frost layer of thickness $\delta_f(t)$ growing on both sides of the extended surface.

4.1. Governing equations

For cylindrical geometry, Eqs. (1), (2), and (4) can be written as (assuming heat transfer only in the r direction for the fin, and in the r and z directions for the frost layer):

$$\frac{\partial T_F}{\partial t}=\frac{k_{eff}}{\rho_FC_Fd}\left.\frac{\partial T_f}{\partial z}\right|_{z=0}+\frac{k_F}{\rho_FC_F}\left[\frac{\partial^2T_F}{\partial r^2}+\frac{1}{r}\frac{\partial T_F}{\partial r}\right]\tag{53}$$

$$\frac{\partial T_f}{\partial t}=\frac{\dot{m}h_{sg}}{\rho_fC_f}+\frac{1}{\rho_fC_f}\left[\frac{\partial}{\partial z}\left(k_{eff}\frac{\partial T_f}{\partial z}\right)+\frac{1}{r}\frac{\partial}{\partial r}\left(k_{eff}r\frac{\partial T_f}{\partial r}\right)\right]\tag{54}$$

$$\frac{\partial}{\partial t}\left[\rho_v(1-\varepsilon_\beta)\right]=\frac{\partial}{\partial z}\left(D_{eff}\frac{\partial\rho_v}{\partial z}\right)+\frac{1}{r}\frac{\partial}{\partial r}\left(D_{eff}r\frac{\partial\rho_v}{\partial r}\right)-\dot{m}\tag{55}$$

4.2. Initial conditions

Assuming that the temperature profile in the fin reaches steady state before frost formation begins, we have [15]

$$\begin{aligned}T_F(r,t=0)=&T_\infty-(T_\infty-T_b)\\&\times\frac{K_1(m_Fr_2)I_0(m_Fr)+K_0(m_Fr)I_1(m_Fr_2)}{K_1(m_Fr_2)I_0(m_Fr_1)+K_0(m_Fr_1)I_1(m_Fr_2)}\end{aligned}\tag{56}$$

$$T_f(r,z,t=0)=T_F(r,t=0)\tag{57}$$

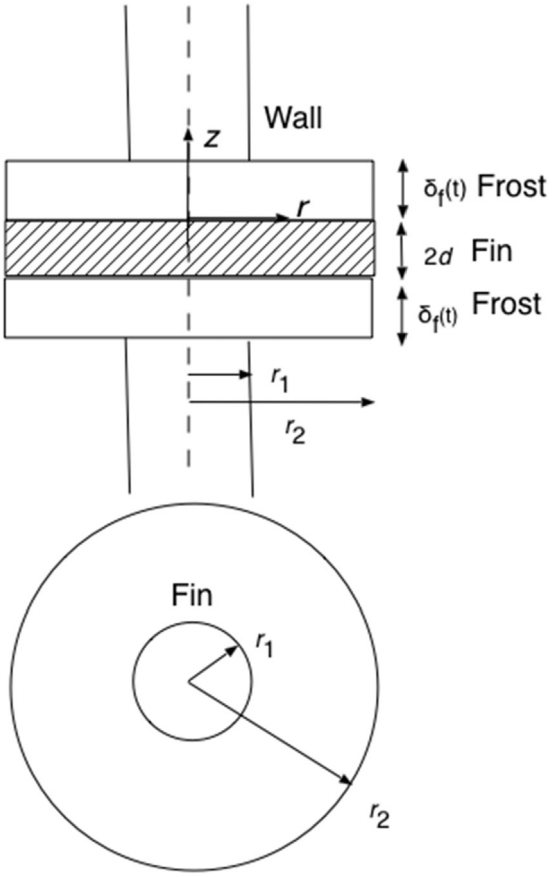

Fig. 2. Schematic diagram of an annular fin showing frost formation.

$$\delta_f(t=0)=\delta_0 \tag{58}$$

$$\varepsilon_\beta(t=0)=\varepsilon_{\beta 0} \tag{59}$$

$$\rho_v(r,z,t=0)=\rho_{v_{sat}}(T_F) \tag{60}$$

4.3. Boundary conditions

For the fin we can write

$$T_F|_{r=r_1}=T_b \tag{61}$$

$$\left.\frac{\partial T_F}{\partial r}\right|_{r=r_2}=0 \tag{62}$$

At the interface between the fin and the frost layer we have

$$T_f|_{r,z=0}=T_F(r) \tag{63}$$

$$\left.\frac{\partial \varepsilon_\beta}{\partial z}\right|_{r,z=0}=0 \tag{64}$$

$$\left.\frac{\partial \rho_v}{\partial z}\right|_{r,z=0}=0 \tag{65}$$

At the interface between the frost layer and the air we have

$$k_{eff}\left.\frac{\partial T_f}{\partial z}\right|_{r,z=\delta_f}=h\left(T_\infty-T_f|_{r,z=\delta_f}\right)+h_{sg}\rho_f\Big|_{r,z=\delta_f}\frac{d\delta_f}{dt} \tag{66}$$

$$\left.\frac{\partial \varepsilon_\beta}{\partial z}\right|_{r,z=\delta_f}=0 \tag{67}$$

$$D_{eff,s}\left.\frac{\overline{\partial \rho_v}}{\partial z}\right|_{r,z=\delta_f}+\rho_f\Big|_{r,z=\delta_f}\frac{d\delta_f}{dt}=h_m\left(\rho_{v,\infty}-\overline{\rho_v}|_{r,z=\delta_f}\right) \tag{68}$$

$$\rho_v|_{r,z=\delta_f}=(1+S)\rho_{v_{sat}}\left(T_f|_{r,z=\delta_f}\right) \tag{69}$$

At the fin base ($r = r_1$) we have

$$T_f|_{r=r_1,z}=T_b \tag{70}$$

$$\left.\frac{\partial \varepsilon_\beta}{\partial r}\right|_{r=r_1,z}=0 \tag{71}$$

$$\left.\frac{\partial \rho_v}{\partial r}\right|_{r=r_1,z}=0 \tag{72}$$

At the fin tip ($r = r_2$) we have

$$\left.\frac{\partial T_f}{\partial r}\right|_{r=r_2,z}=0 \tag{73}$$

$$\left.\frac{\partial \varepsilon_\beta}{\partial r}\right|_{r=r_2,z}=0 \tag{74}$$

$$\rho_v|_{r=r_2,z}=(1+S)\rho_{v_{sat}}\left(T_f|_{r=r_2,z}\right) \tag{75}$$

4.4. Dimensionless coordinates

Define a new dimensionless radial coordinate as:

$$\gamma=\frac{r-r_1}{r_2-r_1} \tag{76}$$

For convenience, in this case we define dimensionless temperatures as:

$$\Theta_f(t,\gamma,\eta)=\frac{T_\infty-T_f(t,\gamma,\eta)}{T_\infty-T_b}\Theta_F(t,\gamma)=\frac{T_\infty-T_F(t,\gamma)}{T_\infty-T_b} \tag{77}$$

4.5. Modified governing equations

Applying the above, the governing equations become as follows:

4.5.1. Energy equation on the fin

$$\frac{\partial \Theta_F}{\partial t}=\frac{1}{\delta_f\rho_F C_F d}\left(k_{eff}\frac{\partial \Theta_f}{\partial \eta}\right)\Big|_{\eta=0}+\frac{k_F}{\rho_F C_F(r_2-r_1)^2}\times\left[\frac{\partial^2\Theta_F}{\partial\gamma^2}+\frac{r_2-r_1}{(r_2-r_1)\gamma+r_1}\frac{\partial\Theta_F}{\partial\gamma}\right] \tag{78}$$

4.5.2. Energy equation in the frost

$$\frac{\partial \Theta_f}{\partial t}=\frac{\eta}{\delta_f}\frac{d\delta_f}{dt}\frac{\partial\Theta_f}{\partial\eta}-\frac{\alpha_t D_{eff}\rho_v h_{sg}}{\delta_f^2\rho_f C_f(T_\infty-T_b)}+\frac{1}{\delta_f^2\rho_f C_f}\frac{\partial}{\partial\eta}\left(k_{eff}\frac{\partial\Theta_f}{\partial\eta}\right)+\frac{1}{\rho_f C_f(r_2-r_1)^2}\frac{\partial}{\partial\gamma}\left(k_{eff}\frac{\partial\Theta_f}{\partial\gamma}\right)+\frac{k_{eff}}{\rho_f C_f(r_2-r_1)[(r_2-r_1)\gamma+r_1]}\frac{\partial\Theta_f}{\partial\gamma} \tag{79}$$

4.5.3. Continuity equation for ice in the frost

Remains as before, regardless of the change in geometry:

$$\frac{\partial \varepsilon_\beta}{\partial t} = \frac{\alpha_t D_{eff} \rho_v}{\delta_f^2 \rho_\beta} + \frac{\eta}{\delta_f}\frac{d\delta_f}{dt}\frac{\delta \varepsilon_\beta}{\delta \eta} \tag{80}$$

4.5.4. Continuity equation for water vapor in the air

$$\begin{aligned}\frac{\partial \rho_v}{\partial t} &= \frac{\rho_v}{(1-\varepsilon_\beta)}\frac{\partial \varepsilon_\beta}{\partial t} + \frac{\eta}{\delta_f}\frac{d\delta_f}{dt}\frac{\partial \rho_v}{\partial \eta} - \frac{\eta \rho_v}{\delta_f(1-\varepsilon_\beta)}\frac{d\delta_f}{dt}\frac{\partial \varepsilon_\beta}{\partial \eta} \\ &- \frac{\alpha_t D_{eff}\rho_v}{\delta_f^2(1-\varepsilon_\beta)} + \frac{1}{\delta_f^2(1-\varepsilon_\beta)}\frac{\partial}{\partial \eta}\left(D_{eff}\frac{\partial \rho_v}{\partial \eta}\right) \\ &+ \frac{1}{(1-\varepsilon_\beta)(r_2-r_1)^2}\frac{\partial}{\partial \gamma}\left(D_{eff}\frac{\partial \rho_v}{\partial \gamma}\right) \\ &+ \frac{D_{eff}}{(1-\varepsilon_\beta)\{\gamma(r_2-r_1)+r_1\}(r_2-r_1)}\frac{\partial \rho_v}{\partial \gamma}\end{aligned} \tag{81}$$

The time rate of increase of frost layer thickness remains as before:

$$\frac{d\delta_f}{dt} = \frac{h_m\left(\rho_{v,\infty} - \overline{\rho_v}\big|_{\eta=1}\right)}{\rho_f\big|_{\eta=1}} - \frac{D_{eff,s}}{\delta_f \rho_f\big|_{\eta=1}}\left.\frac{\overline{\partial \rho_v}}{\partial \eta}\right|_{\eta=1} \tag{82}$$

Eqs. (78)–(82) form a set of nonlinear, coupled PDEs whose solution must be obtained by a suitable numerical method.

4.6. Orthogonal collocation method

The governing equations must be satisfied at each of the N internal collocation points. The radial derivatives are discretized as follows (illustrated here with the dimensionless temperature, but applicable to other properties)

$$\left.\frac{\partial \Theta_f}{\partial \gamma}\right|_{i,k} = \sum_{j=1}^{N+2} Ar(i,j)\Theta_f(j,k) \quad \left.\frac{\partial^2 \Theta_f}{\partial \gamma^2}\right|_{i,k} = \sum_{j=1}^{N+2} Br(i,j)\Theta_f(j,k) \tag{83}$$

For cylindrical coordinates, when the radial domain includes the origin, there are different equations to calculate the position of the internal collocation points and the derivative matrices **Ar** and **Br** instead of those used for rectangular coordinates for those purposes. However, they do not apply to an annular region such as the one considered in this case. To circumvent this restriction, we defined a dimensionless radial position (γ) in Eq. (76) with a domain from 0 to 1.0; and used the position of the internal collocation points and matrices **A** and **B** corresponding to rectangular coordinates [12]. A quadrature formula to estimate the value of average properties in the radial direction is as follows:

$$\begin{aligned}\overline{\Theta_f}(t,\eta) &= \frac{\int_{r_1}^{r_2} 2\pi r \Theta_f(t,\eta,r)dr}{\int_{r_1}^{r_2} 2\pi r dr} \\ &= \frac{2(r_2-r_1)}{(r_2+r_1)}\int_0^1 \gamma \Theta_f(t,\eta,\gamma)d\gamma + \frac{2r_1}{(r_2+r_1)} \\ &\times \int_0^1 \Theta_f(t,\eta,\gamma)d\gamma\end{aligned} \tag{84}$$

$$\begin{aligned}\overline{\Theta_f}(t,\eta) &\approx \frac{2(r_2-r_1)}{(r_2+r_1)}\sum_{j=1}^{N+2} w_j \gamma_j \Theta_f\left(t,\eta,\gamma_j\right) \\ &+ \frac{2r_1}{(r_2+r_1)}\sum_{j=1}^{N+2} w_j \Theta_f\left(t,\eta,\gamma_j\right)\end{aligned} \tag{85}$$

In Eq. (85), w_j is the quadrature weight corresponding to the root γ_j. The weights are obtained from the MATLAB program given by Do [10].

The governing equations, in terms of orthogonal collocation, become:

$$\begin{aligned}\frac{d\Theta_F(i)}{dt} &= \frac{k_{eff}\big|_{\eta=0}}{\delta_f \rho_F C_F d}\sum_{l=1}^{M+2} Az(i,j)\Theta_f(i,l) + \frac{k_F}{C_F \rho_F (r_2-r_1)^2} \\ &\times \left[\sum_{j=1}^{N+2} Br(i,j)\Theta_F(j) + \frac{r_2-r_1}{\gamma_i(r_2-r_1)+r_1}\sum_{j=1}^{N+2} Ar(i,j)\Theta_F(j)\right]\end{aligned} \tag{86}$$

$$\begin{aligned}\frac{d\Theta_f(i,k)}{dt} &= \frac{\eta_k}{\delta_f}\frac{d\delta_f}{dt}\sum_{l=1}^{M+2} Az(k,l)\Theta_f(i,l) - \frac{\alpha_t D_{eff}(i,k) h_{sg}\rho_v(i,k)}{\rho_f C_f \delta_f^2 (T_\infty - T_b)} \\ &+ \frac{k_{eff}(i,k)}{\rho_f C_f \delta_f^2}\sum_{l=1}^{M+2} Bz(k,l)\Theta_f(i,l) \\ &+ \frac{1}{\rho_f C_f \delta_f^2}\sum_{l=1}^{M+2} Az(k,l)\Theta_f(i,l)\sum_{l=1}^{M+2} Az(k,l)k_{eff}(i,l) \\ &+ \frac{k_{eff}(i,j)}{\rho_f C_f (r_2-r_1)^2}\sum_{j=1}^{N+2} Br(i,j)\Theta_f(j,k) \\ &+ \frac{1}{\rho_f C_f (r_2-r_1)^2}\sum_{j=1}^{N+2} Ar(i,j)\Theta_f(j,k)\sum_{j=1}^{N+2} Ar(i,j)k_{eff}(j,k) \\ &+ \frac{k_{eff}(i,j)}{\rho_f C_f\left[(r_2-r_1)^2\gamma_i + r_1(r_2-r_1)\right]}\sum_{j=1}^{N+2} Ar(i,j)\Theta_f(j,k)\end{aligned} \tag{87}$$

$$\frac{d\varepsilon_\beta(i,k)}{dt} = \frac{\alpha_t D_{eff}(i,k)\rho_v(i,k)}{\delta_f^2 \rho_\beta} + \frac{\eta_k}{\delta_f}\frac{d\delta_f}{dt}\sum_{l=1}^{M+2} Az(k,l)\varepsilon_\beta(i,l) \tag{88}$$

$$\begin{aligned}\frac{d\rho_v(i,k)}{dt} &= \frac{\rho_v(i,k)}{[1-\varepsilon_\beta(i,k)]}\frac{\partial \varepsilon_\beta(i,k)}{\partial t} + \frac{\eta_k}{\delta_f}\frac{d\delta_f}{dt}\sum_{l=1}^{M+2} Az(k,l)\rho_v(i,l) \\ &- \frac{\eta_k \rho_v(i,k)}{\delta_f[1-\varepsilon_\beta(i,k)]}\frac{d\delta_f}{dt}\sum_{l=1}^{M+2} Az(k,l)\varepsilon_\beta(i,l) \\ &- \frac{\alpha_t D_{eff}(i,k)\rho_v(i,k)}{[1-\varepsilon_\beta(i,k)]\delta_f^2} + \frac{1}{[1-\varepsilon_\beta(i,k)]\delta_f^2} \\ &\times \left(\sum_{l=1}^{M+2} Az(k,l)\rho_v(i,l)\sum_{l=1}^{M+2} Az(k,l)D_{eff}(i,l) + D_{eff}(i,k)\sum_{l=1}^{M+2} Bz(k,l)\rho_v(i,l)\right) \\ &+ \frac{1}{[1-\varepsilon_\beta(i,k)](r_2-r_1)^2}\sum_{j=1}^{N+2} Ar(i,j)\rho_v(j,k)\sum_{j=1}^{N+2} Ar(i,j)D_{eff}(j,k) \\ &+ \frac{D_{eff}(i,k)}{[1-\varepsilon_\beta(i,k)](r_2-r_1)^2}\sum_{j=1}^{N+2} Br(i,j)\rho_v(j,k) \\ &+ \frac{1}{[1-\varepsilon_\beta(i,k)]\left[\gamma_i(r_2-r_1)^2 + r_1(r_2-r_1)\right]}\sum_{j=1}^{N+2} Ar(i,j)\rho_v(j,k)\end{aligned} \tag{89}$$

Eq. (82) is written in terms of orthogonal collocation as:

$$\begin{aligned}\frac{\partial \delta_f}{\partial t} &= \frac{h_m\left[\rho_{v,\infty} - \overline{\rho_v}(N+2)\right]}{\rho_\beta \overline{\varepsilon_\beta}(N+2)} \\ &- \frac{D_{eff,s}}{\delta_f \rho_\beta \overline{\varepsilon_\beta}(N+2)}\overline{\sum_{j=1}^{N+2} Az(N+2,j)\rho_v(i,N+2)}\end{aligned} \tag{90}$$

The average values in Eq. (90) are evaluated using Eq. (85). The frost density at any point is approximated with the product of the ice density and the ice volume fraction, as justified above. The boundary conditions must also be expressed in terms of the collocation points.

Eqs. (86)–(90), with initial conditions given by Eqs. (56)–(60), constitute an initial value problem (IVP) that can be approximately solved using the ode15s program of MATLAB.

5. Results and discussion

5.1. Rectangular fins

In order to calculate the convective mass- and heat-transfer coefficients, details about the geometric configuration of the fin arrangement must be specified. Since we will test our model with the experimental data obtained by Chen et al. [6] and Kim et al. [20], a similar configuration will be used, as shown in Fig. 3. The air will flow through a rectangular channel formed by two successive fins, the cold base wall, and an insulated lid. The flow through the channel is turbulent with Reynolds numbers between 3000 and 10,000. The Gnielinski [13] correlation applies under these conditions, and is used to estimate the heat-transfer coefficient:

$$Nu_D = \frac{(f/8)(Re_D - 1000)Pr}{1 + 12.7(f/8)^{1/2}\left(Pr^{2/3} - 1\right)} \tag{91}$$

Assuming heat and mass transfer similarity ($j_D = j_H$) for this slowly varying heat and mass transfer process allows calculation of the mass-transfer coefficient [2].

The orthogonal collocation method usually achieves great accuracy with a small number of collocation points. For dependent variables that change smoothly with position, $N = 2$, (where N is the number of internal collocation points) is usually sufficient. The collocation roots, quadrature weights, and the first- and second-order derivative matrices are easily obtained from the literature for a given geometry and N value. Table 1 shows the results obtained for $N = 2$ obtained using in this case the MATLAB program given by Do [10].

To fix the domain of the space coordinates between zero and one, we use the front-fixing method. Then, the space-discretized set of equations is integrated in time to follow the changing position of the moving boundary. This procedure eliminates the need to use a pseudo-steady-state approximation frequently used by researchers in this area. The method presented here can be used for many problems in which a boundary is moving.

The degree of super saturation (S) required for frost formation is a very important parameter in our formulation. Fig. 4 shows the importance of the value of S when trying to simulate the experimental results on the variation of the frost layer thickness with time obtained by Chen et al. [6]. The experimental conditions used by these researchers are summarized in Table 2. The experimental values of frost thickness at the end of 4 h, shown in Fig. 4, correspond to 91 measurements taken at different positions on the rectangular fin. Assuming saturation at the interface ($S = 0$), the model significantly overestimates the frost layer development at all times. This can be explained from a mass transfer point of view. The driving force for water-vapor transfer rate from the humid air surrounding the frost to the air inside the porous solid layer is the difference between the water-vapor partial pressure in the bulk of the humid air and the corresponding partial pressure in the air filling the pores at the air-frost interface. Assuming that the air in the pores at the interface is saturated results in overestimating this driving force. As mentioned before—as far as we know—there is no way of predicting the value of S; therefore, it must be estimated by comparing the model predictions for different values of S to experimental results. For the set of experimental conditions used by Chen et al. [6], simulations with a value of $S = 15\%$ agree well with the average value of the experimental data.

Fig. 5 shows the variation of the frost layer thickness with time obtained by Kim et al. [20]. The experimental conditions used by these researchers are also summarized in Table 2. Simulations with a value of $S = 8.0\%$ agree well with the experimental data, as Fig. 5 shows. Fig. 6 shows the temperature distribution on the surface of the fin at the end of a frost formation period of 4 h for the experimental conditions described by Chen et al. [6]. The final distribution predicted by the model (with $S = 15\%$) agrees well with the experimental data. Fig. 7 shows the temperature distribution on

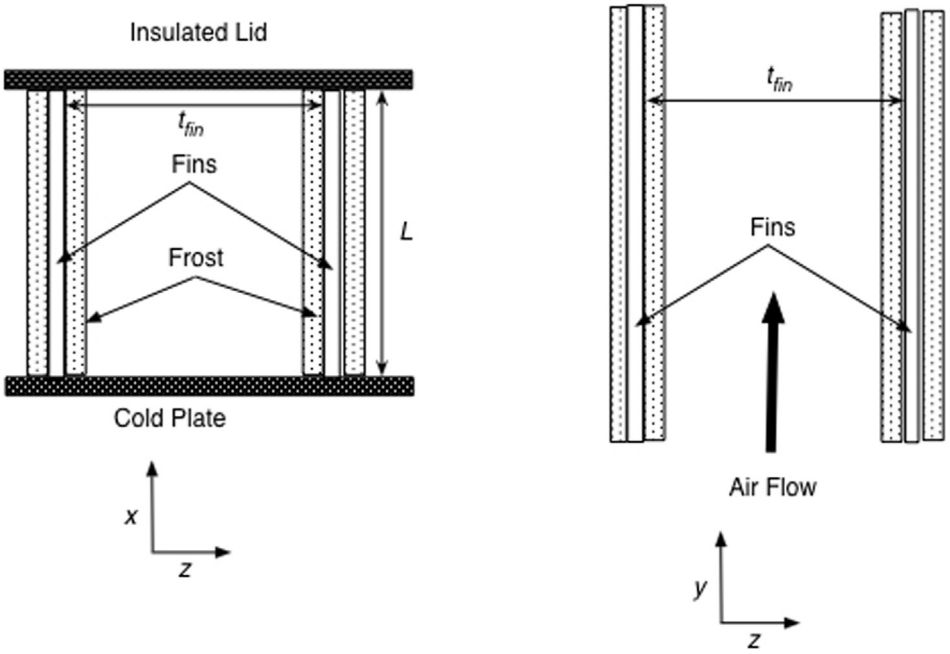

Fig. 3. Schematic diagram of frost-covered rectangular heat exchanger fins, elevation and plan views.

Table 1
Roots, weights, and matrices for $N = 2$, rectangular geometry [10].

i	η_i[a]	w_i[b]	**A**[c]				**B**[d]			
1	0.0	0.044	−6.0	8.090	−3.090	1.0	20.0	−38.54	28.54	−10.0
2	0.276	0.435	−1.618	0.0	2.236	−0.618	11.71	−20.0	10.0	−1.71
3	0.724	0.435	0.618	−2.236	0.0	−1.618	−1.71	10.0	−20.0	11.71
4	1.0	0.087	−1.0	3.090	−8.090	6.0	−10.0	28.54	−38.54	20.0

[a] Roots of the $(N + 2)$ degree Jacobi orthogonal polynomial.
[b] Weights used in quadrature formula, Eq. (47).
[c] Discretization first-derivative matrix, Eqs. (45) and (46).
[d] Discretization second-derivative matrix, Eqs. (45) and (46).

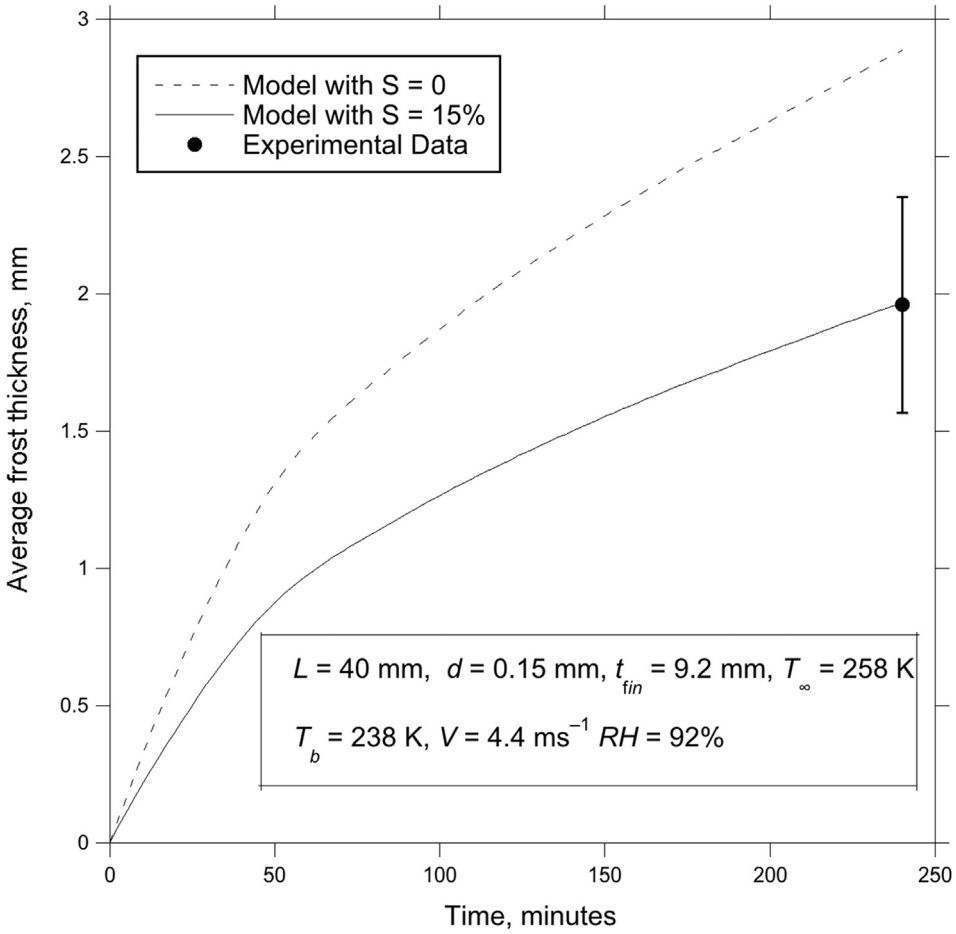

Fig. 4. Variation of frost thickness with time. Experimental result shown is the average of 91 measurements of frost thickness at different points on the fin surface after 4 h [6].

Table 2
Experimental test conditions used for rectangular fins.

Parameter	Chen et al. [6]	Kim et al. [20]
Fins material	Aluminum alloy	Aluminum alloy
Fins length, L (mm)	40.0	70.0
Fins half-thickness, d (mm)	0.15	0.5
Fins spacing, t_{fin} (mm)	9.2	40[a]
Air dry-bulb temperature, °C	−15.0	7.0
Cold plate temperature, °C	−35.0	−20.0
Average air velocity, m s^{-1}	4.4	1.0
Humidity of the air	92% RH	0.00464 kg × kg^{-1}
Time of frost growth, min	240	90

[a] Estimated from schematic diagram of Kim et al. [20].

the surface of the fin at the end of a frost formation period of 90 min for the experimental conditions described by Kim et al. [20]. The final distribution predicted by the model (with $S = 8.0\%$) agrees well with the experimental data.

The effect of frost growth on the rate of heat transfer through the fin can be ascertained using the model results to calculate the variation with time of a dimensionless heat flux, $Q(t)$, defined for a rectangular fin as

$$Q(t) = \frac{q(x=0,t)}{q(x=0,t=0)} = \frac{\sum_{j=1}^{N+2} Ax(1,j)\theta_F(j)}{m_F L \tanh(m_F L)} \tag{92}$$

This is the ratio of the heat flux from the fin to the cold wall at any time during the frost formation period divided by the corresponding heat flux before frost formation starts.

Fig. 8 shows the variation of the dimensionless heat flux with time for the experimental conditions used by Chen et al. [6]. The model predicts the general trend displayed by the experimental

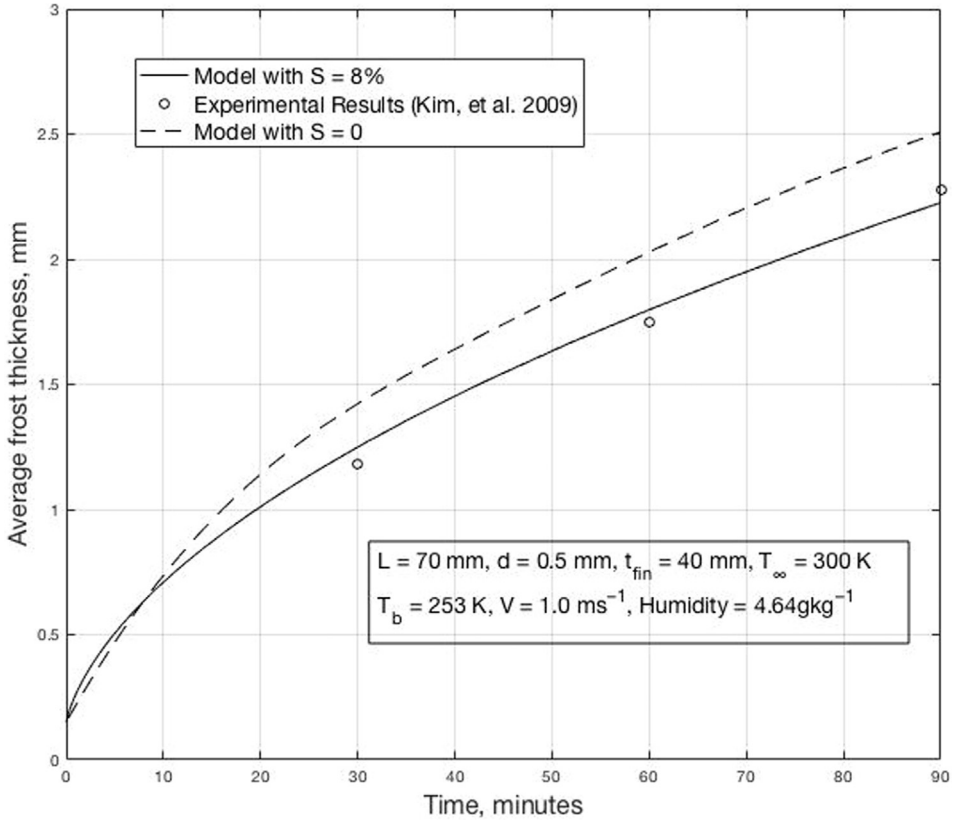

Fig. 5. Variation of frost thickness with time. Experimental results are from Kim et al. [20]. Each point corresponds to the average of 4 measurements at different points on the fin.

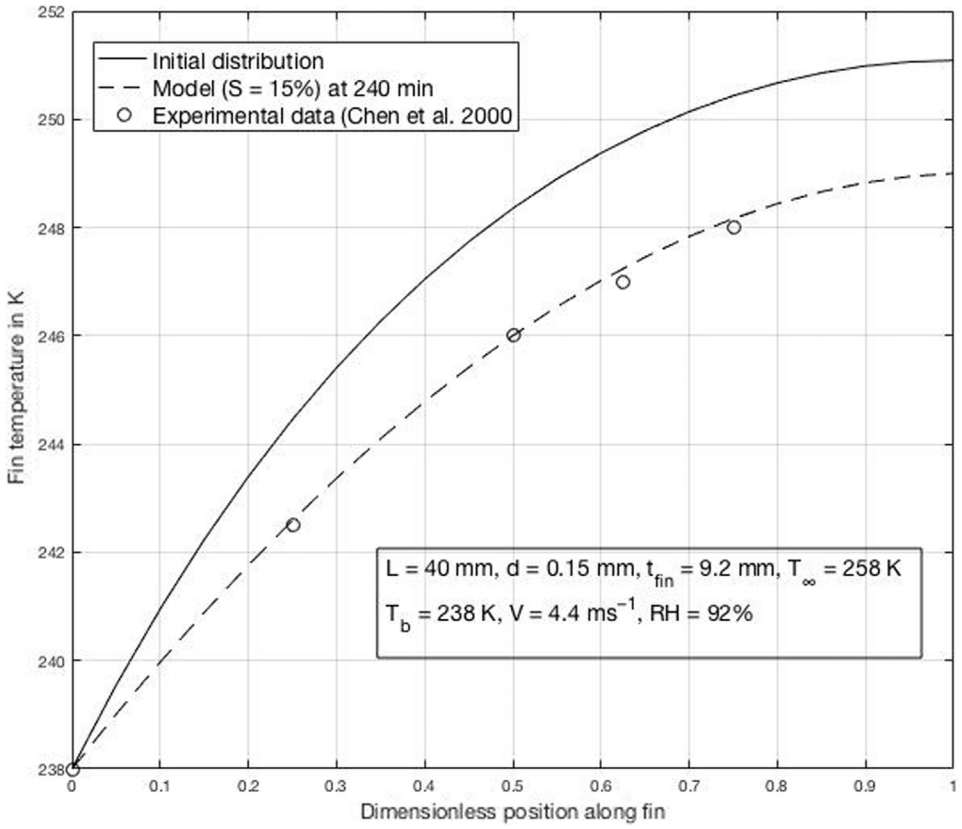

Fig. 6. Temperature distribution on the surface of the fin. The experimental data from Chen et al. [6] were measured at the end of 4 h.

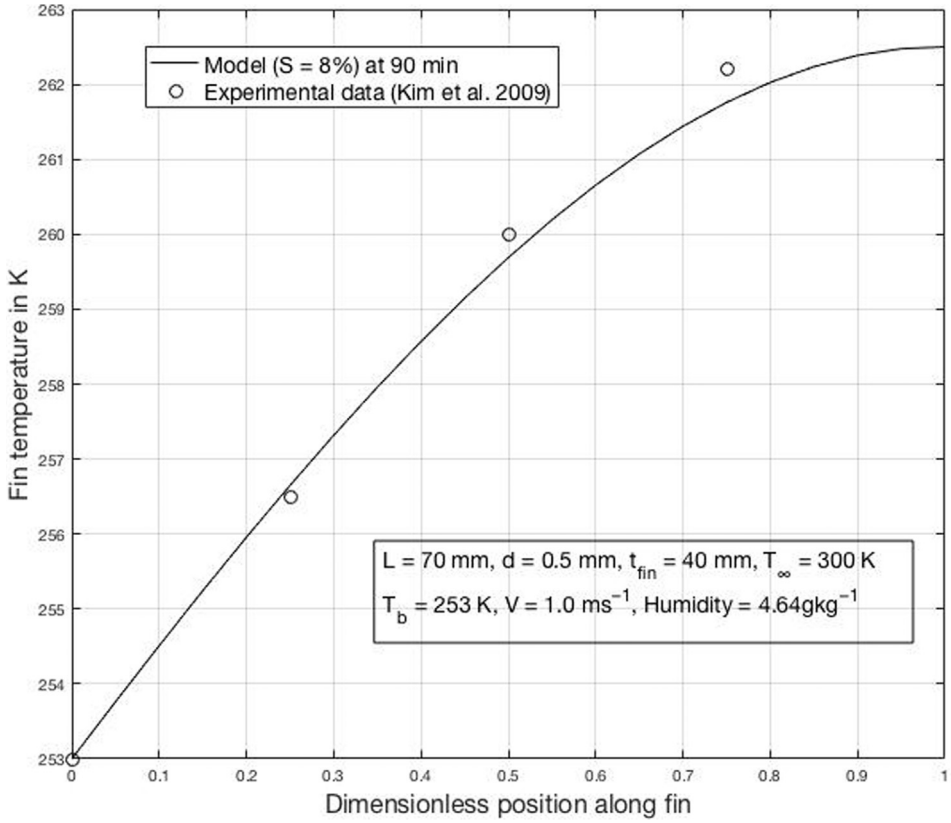

Fig. 7. Temperature distribution on the surface of the fin. The experimental data from Kim et al. [20] were measured at the end of 90 min.

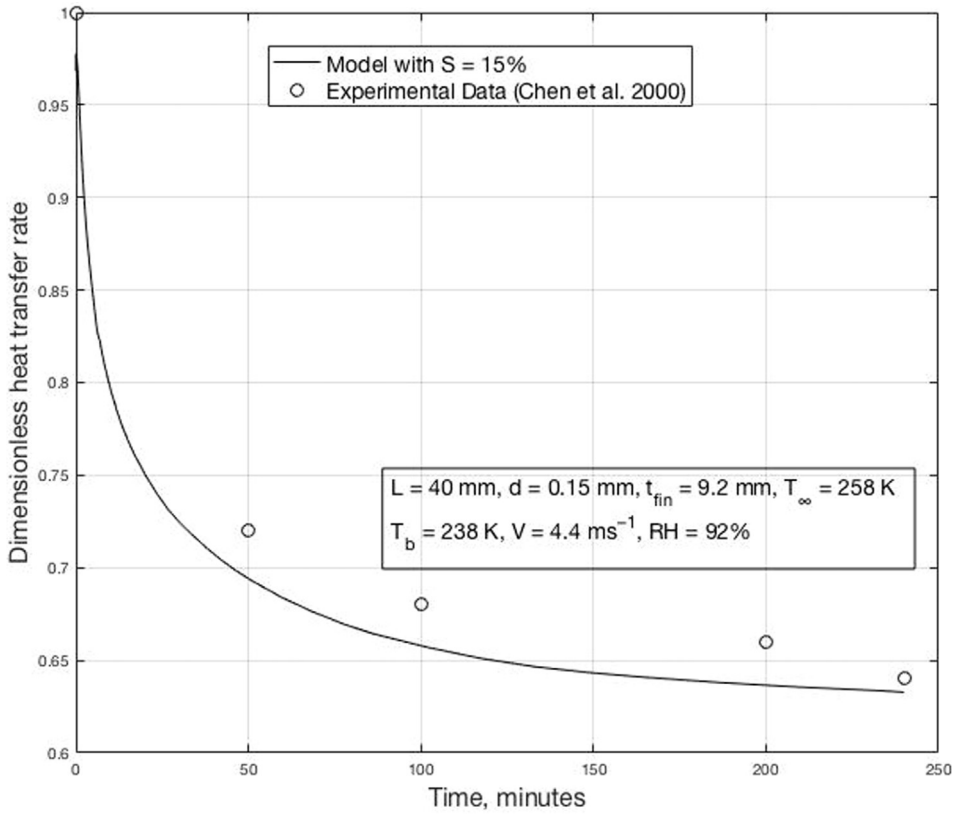

Fig. 8. Dimensionless heat transfer rate as a function of time. Experimental data are from Chen et al. [6].

data. However, it consistently over predicts the insulating effect of the accumulating frost layer. The reason for this is that the model assumes constant values of the convective heat- and mass-transfer coefficients. Actually, these coefficients will tend to increase as frost accumulation partially blocks the airflow path and, for a constant airflow rate, the gas velocity increases. The increase in convective heat and mass flow at the air-frost interface partially offsets the insulating effect of the frost layer. However, as Fig. 8 shows, the net effect of frost formation is a significant heat flux reduction over time. [Kim et al. [20] did not measure the heat flux variation with time in their experimental setup.]

Table 3
Experimental test conditions used for annular fins.

Parameter	Forced convection[a]	Natural convection[b]
Fins material	Aluminum	Aluminum
Fins diameter, (mm)	23.0	56.0
Tube outside diameter, (mm)	8.0	25.4
Fins half-thickness, (mm)	0.075	0.2
Fins spacing, (mm)	10.0	2.0
Air dry-bulb temperature, °C	5.0	18.0/22.0
Cold plate temperature, °C	−15.0	− 9.0
Humidity of the air, %	50/60/70/80	35/45

[a] Lee et al. [23].
[b] Mahdavi and Yaghoubi [27].

5.2. Annular fins

In order to calculate the convective mass- and heat-transfer coefficients, details about the geometric configuration of the finned-tubes arrangement must be specified. Since we will test our model with the experimental data obtained by Lee et al. [23] and Mahdavi and Yaghoubi [27], a similar configuration will be used, as shown in Fig. 9. Lee et al. [23] worked under forced convection conditions, while Mahdavi and Yaghoubi [27] did it under natural convection conditions. Table 3 summarizes the experimental conditions used in both works.

Forced Convection

Lee et al. [23] studied experimentally frost growth on a large-pitch fin-tube heat exchanger for low temperature heat pumps. They worked with fin separations ranging from 4.0 to 12.0 mm. These are significantly larger than the fin pitch of heat exchangers used for residential and commercial systems (usually in the range of 1.4–2.0 mm). This is because the frosting problem is very important in this case since frost growth blocks the air path, decreasing the airflow rate if the fin separation is not large enough.

Lee et al. [22] developed a heat-transfer coefficient correlation for an inline finned-tube alignment, for fin pitches of 7.5–15.0 mm. We used their correlation to estimate the heat-transfer coefficient for the experimental conditions of Lee et al. [23] summarized in Table 3. Assuming heat and mass transfer similarity for this slowly varying heat and mass transfer process allows calculation of the mass-transfer coefficient [2].

Fig. 10 shows the variation of the frost layer thickness with time obtained by Lee et al. [23] at a relative humidity of 70%. Simulations with a value of $S = 11.0\%$ agree well with the experimental data. (In all simulations of annular fins we used $N = 2$ in both the radial and axial coordinates.)

The concept of a dimensionless heat flux introduced in Eq. (92) is modified here for an annular fin as

$$Q(t) = \frac{q(r = r_1, t)}{q(r = r_1, t = 0)} = \frac{-\sum_{i=1}^{N+2} Ar(1,i)\Theta_F(i)}{m_F(r_2 - r_1)\frac{K_1(m_F r_1)I_1(m_F r_2) - K_1(m_F r_2)I_1(m_F r_1)}{K_1(m_F r_2)I_0(m_F r_1) + K_0(m_F r_1)I_1(m_F r_2)}} \tag{93}$$

Fig. 11 shows the variation of the dimensionless heat flux with time for the experimental conditions used by Lee et al. [23] at a relative humidity of 80% as predicted by our model. It shows that initially the latent heat transfer due to ice deposition makes Q much higher than 1.0, but then it decreases monotonically as the frost layer thickness increases. Eventually, the insulating effect of the presence of the frost layer becomes more pronounced and the heat flux is reduced by more than 40%. Lee et al. [23] did not measure the heat flux; therefore, there are no experimental data in this case to corroborate the model predictions.

5.2.1. Natural convection

Mahdavi and Yaghoubi [27] studied experimentally frost deposition over a compact finned-tube by natural convection. The fins were annular, with a small fin pitch (2 mm), common in air-cooled heat exchangers and some refrigerated evaporators. Chen and Hsu [7] presented various correlations to estimate the heat transfer coefficient on annular-finned tube heat exchangers in natural convection. We used their correlation to estimate the heat-transfer coefficient for the experimental conditions of Mahdavi and Yaghoubi [27] summarized in Table 3. Assuming heat and

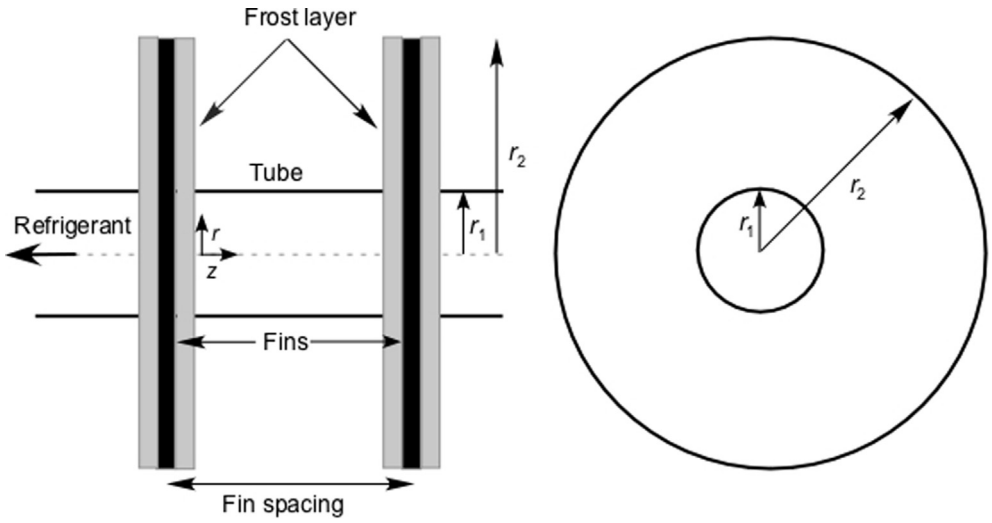

Fig. 9. Schematic diagram of an annular finned-tube showing frost formation on the fin surfaces.

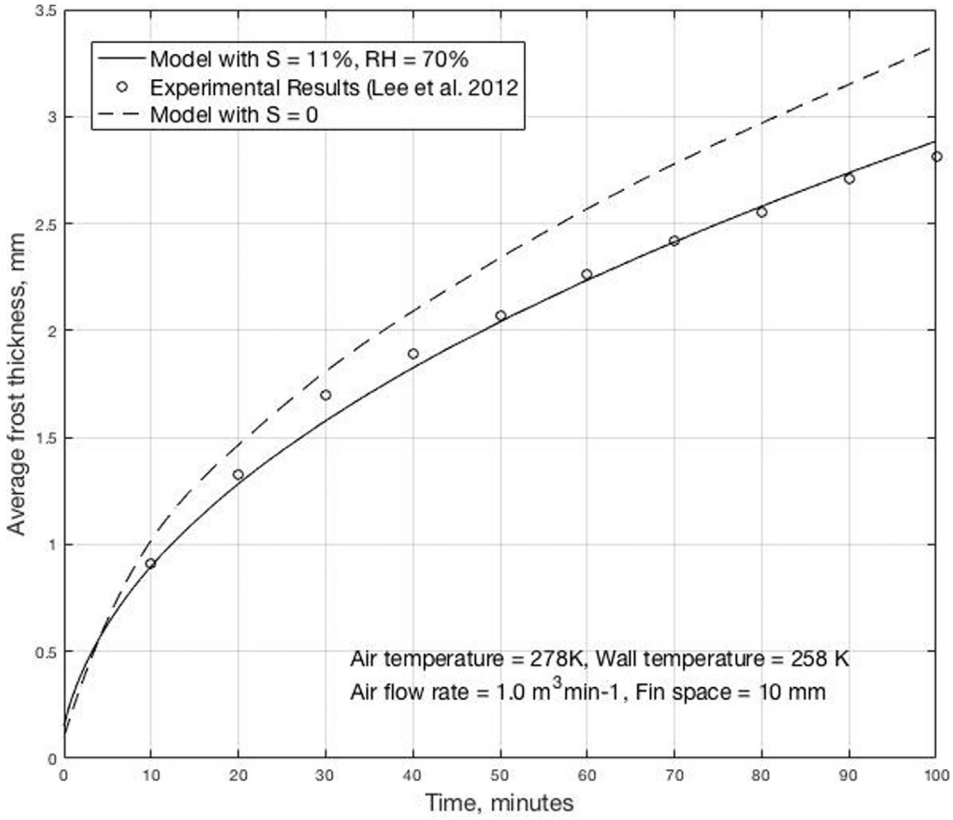

Fig. 10. Variation of frost thickness with time under forced convection. Data are from Lee et al. [23].

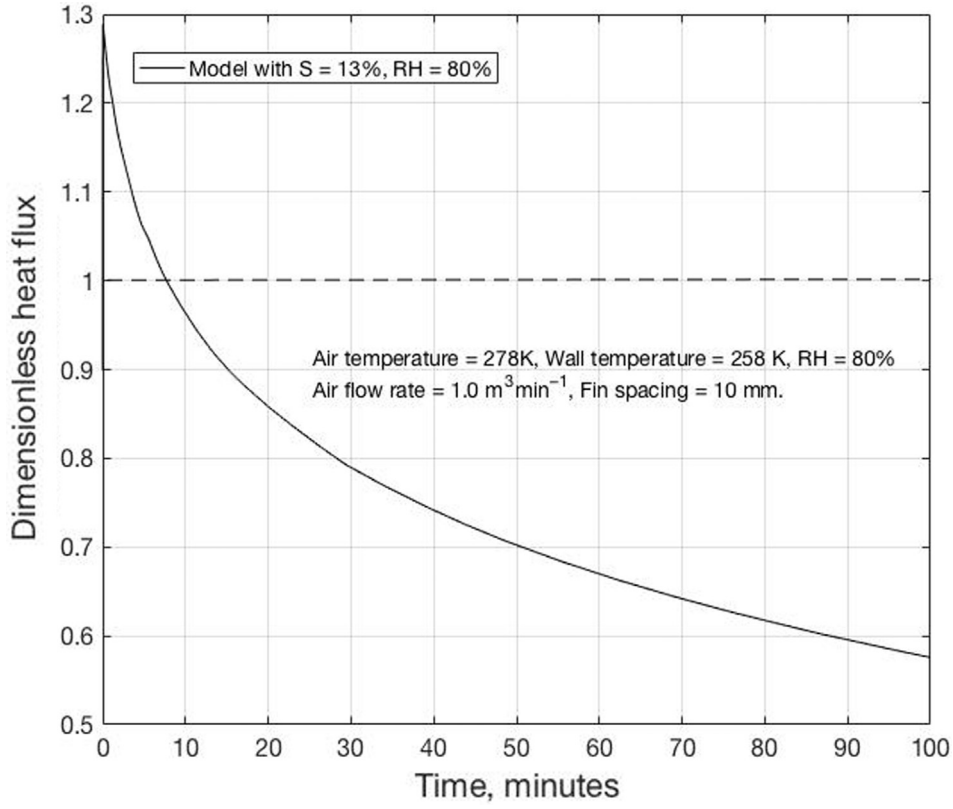

Fig. 11. Variation with time of the dimensionless heat flux at the fin base for the experimental conditions of Lee et al. [23].

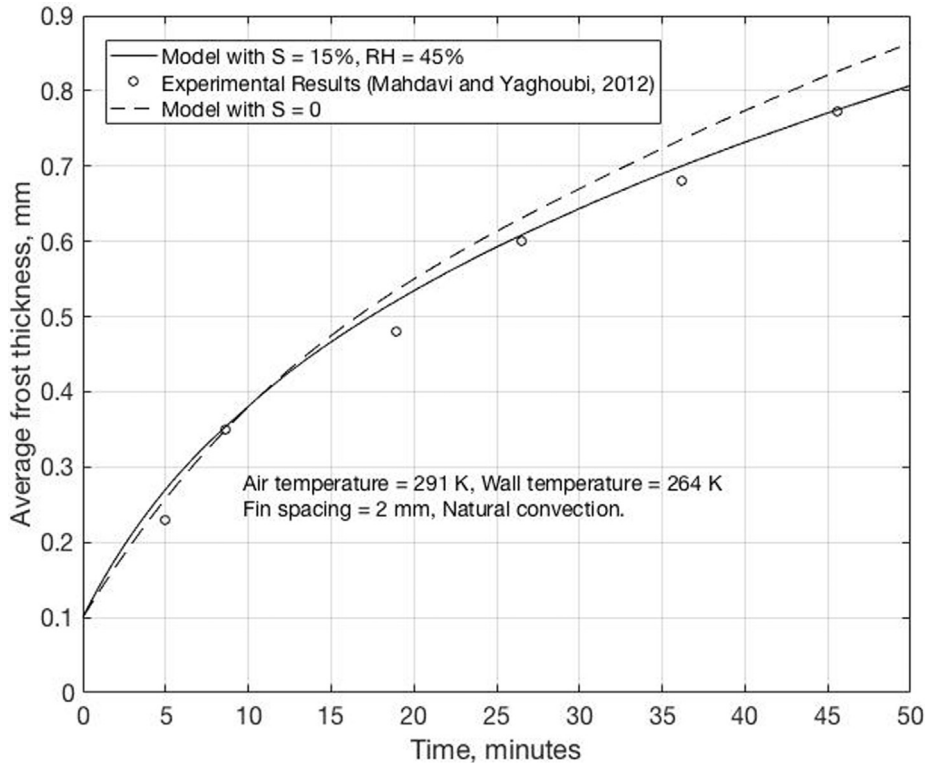

Fig. 12. Variation of frost thickness with time, under natural convection conditions, relative humidity of 45%. Data are from Mahdavi and Yaghoubi [27].

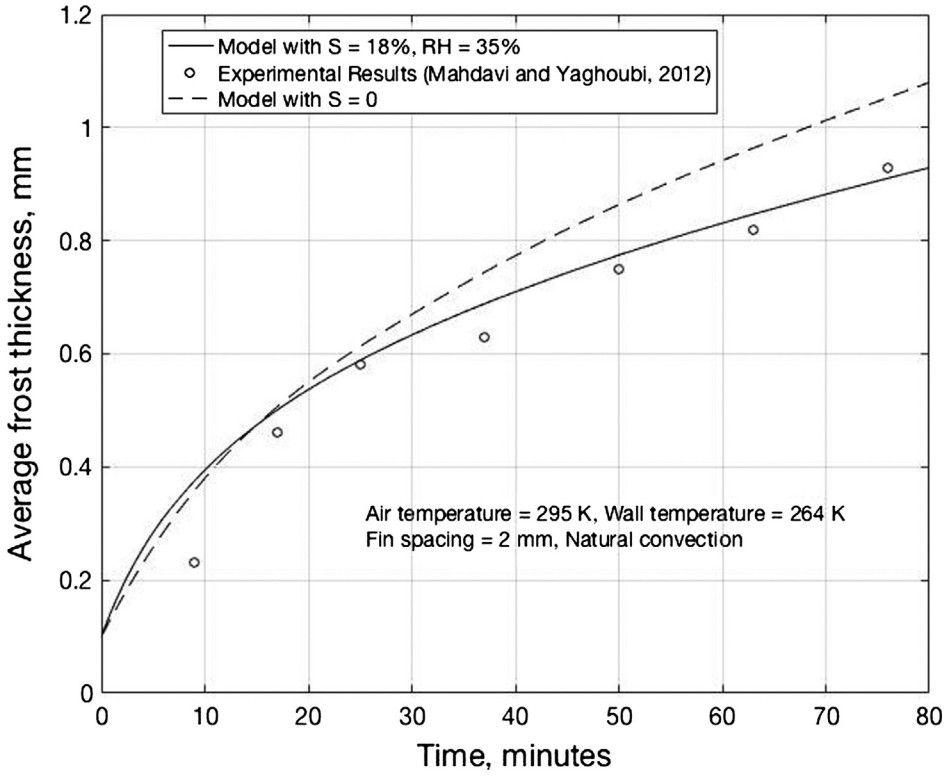

Fig. 13. Variation of frost thickness with time, under natural convection conditions, relative humidity of 35%. Data are from Mahdavi and Yaghoubi [27].

mass transfer similarity allowed calculation of the mass-transfer coefficient [2].

Fig. 12 shows the effect of the value of S when trying to simulate frost growth under the experimental set-up used by Mahdavi and Yaghoubi [27] at a relative humidity of 45%, air temperature of 291 K, and natural convection. Simulations with a value of $S = 15\%$ agree well with the experimental data, as Fig. 12 shows. Fig. 13 shows similar results for a relative humidity of 35%. In that case, the best estimate of the super saturation degree is $S = 18\%$.

Fig. 12 shows that at a time of 50 min, for a relative humidity of 45%, the frost layer has grown to about 0.8 mm. Since the fin spacing is just 2.0 mm, the area for airflow has therefore been reduced by 80%. For the conditions illustrated in Fig. 13, at a relative humidity of 35%, it takes about 60 min for a similar blockage to occur. The researchers observed that after about 30–200 min, depending on the various controlling parameters, complete blockage of the space between the fins occur [27] After that point, frost continues to grow, but in the radial direction and the fin-tube arrangement behaves as a solid cylinder.

6. Conclusions

We introduced in this work a new computational scheme—first suggested by Benítez and Sherif [3] to model frost formation on flat plates—to numerically solve the transient equations that describe frost formation over rectangular and annular fins with humid air flowing over the fin surface. The methodology presented uses the front-fixing method to handle the moving boundary. The boundary is fixed in the newly defined set of coordinates, but additional differential terms modify the original governing equations. The spatial derivatives of the modified governing equations are discretized through the orthogonal collocation method with N internal points in both position coordinates. The ode15s program of MATLAB is used to approximate the solution of the set of initial value equations resulting from the discretization process.

Temporal variations of the frost thickness, frost surface temperature, and heat flux through the fin were predicted and the results compared to experimental data available in the literature. Even though for illustration purposes a small number of collocation points ($N = 2$) were chosen, the model predictions were very close to the experimental results observed. The program also predicted spatial and temporal variations of other frost properties such as temperature, ice volumetric fraction, density, and water vapor density in a manner similar to that presented for a flat plate in our previous work [3]. Those results are not shown here to keep this paper within a reasonable length, and because there were no experimental data in the literature to compare them to.

The proposed computational scheme was shown to accurately describe the dynamics of frost formation on rectangular and annular fins, even though a very simple grid consisting of only 16 points was used to spatially discretize the PDEs. No special software was needed to run the model, easily programmed in MATLAB. Given the prevalence of these types of fins in refrigeration applications, this analytical approach could be a significant contribution.

In all data sets modeled, it was found that a certain degree of super saturation at the frost-air interface must be included in the model to accurately predict frost growth. The absolute deviation between the model predictions and the experimental data were of the order of 1.0% or less, provided that the super saturation degree at the frost-air interface was properly adjusted. Even though the mathematical description of the annular fins was significantly more complex than for the rectangular fins due to the variable cross-sectional area for heat transfer, the computational scheme presented in this work could handle the added degree of difficulty.

Conflict of interest

This research did not receive any specific grant from funding agencies in the public, commercial, or not-for-profit sectors.

Appendix A. Supplementary material

Supplementary data associated with this article can be found, in the online version, at https://doi.org/10.1016/j.ijheatmasstransfer.2019.02.005.

References

[1] M.A.S. Barrozo, H.M. Henrique, D.J.M. Sartori, J.T. Freire, The use of the orthogonal collocation method on the study of the drying kinetics of soybean seeds, J. Stored Prod. Res. 42 (2006) 348–356.
[2] J. Benítez, Principles and Modern Applications of Mass Transfer Operations, third ed., John Wiley and Sons, Hoboken, NJ, 2017.
[3] T. Benítez, S.A. Sherif, Modeling spatial and temporal frost formation with distributed properties on a flat plate using the orthogonal collocation method, Int. J. Refrig. 76 (2017) 193–205.
[4] E.C. Biscaia, M.B. Mansur, A. Salum, R.M.Z. Castro, A moving boundary problem and orthogonal collocation in solving a dynamic liquid surfactant membrane model including osmosis and breakage, Braz. J. Chem. Eng. 18 (2) (2001) 1–18.
[5] H. Chen, L. Thomas, R.W. Besant, Measurements of frost characteristics on heat exchanger fins - Part II: data and analysis, ASHRAE Trans. 105 (1999) 294–302.
[6] H. Chen, L. Thomas, R.W. Besant, Modeling frost characteristics on heat exchanger fins - Part I: numerical model, ASHRAE Trans. 106 (2000) 357–367.
[7] H.-T. Chen, W.-L. Hsu, Estimation of heat transfer coefficient on the fin of annular-finned tube heat exchangers in natural convection for various fin spacing, Int. J. Heat Mass Transfer 50 (2007) 1750–1761.
[8] J. Crank, Free and Moving Boundary Problems, Oxford University Press, New York, 1984.
[9] M.A. Dietenberger, Generalized correlation of the water frost thermal conductivity, Int. J. Heat Mass Transfer 26 (4) (1983) 607–619.
[10] D.D. Do, Adsorption Analysis: Equilibria and Kinetics, Imperial College Press, London, 1998.
[11] A.F. Emery, B.L. Siegel, Experimental measurements of the effects of frost formation on heat exchanger performance, in: R.V. Arimilli, D.E. Beasley, S. Sengupta, S.A. Sherif, R.G. Watts (Eds.), Proceedings of 5th AIAA/ASME Thermophysics and Heat Transfer Conference. In Heat and Mass Transfer in Frost and Ice Packed Beds and Environmental Discharges, ASME HTD 139, Book No. H00592, New York, 1990, pp. 1–7.
[12] B. Finlayson. Professor Emeritus of Chemical Engineering, University of Washington, Seattle, Washington, 2017 (Personal communication).
[13] V. Gnielinski, New equations for heat and mass-transfer in turbulent pipe and channel flow, Int. Chem. Eng. 16 (2) (1976) 359–368.
[14] K. Hirbodi, M. Yaghoubi, Experimental investigation of natural dehumidification over an annular finned-tube, Exp. Thermal and Fluid Sci. 57 (2014) 128–144.
[15] F.P. Incropera, D.P. Dewitt, Introduction to Heat Transfer, fourth ed., John Wiley and Sons, New York, 2002.
[16] B.W. Jones, J.D. Parker, Frost formation with varying environmental parameters, J. Heat Transfer 97 (1975) 255–259.
[17] M. Kandula, Frost growth and densification in laminar flow over flat surfaces, Int. J. Heat Mass Transfer 54 (2011) 3719–3731.
[18] K. Kim, J. Kim, K. Lee, Characteristics of frost formation on two-dimensional fins and its empirical correlations, Int. J. Heat Mass Transfer 53 (2010) 2670–2675.
[19] D. Kim, C. Kim, K.S. Lee, Frosting model for predicting macroscopic and local frost behaviors on a cold plate, Int. J. Heat Mass Transfer 82 (2015) 135–142.
[20] J. Kim, K. Lee, S. Yook, Frost behavior on a fin considering the heat conduction of heat exchanger fins, Int. J. Heat Mass Transfer 52 (2009) 2581–2588.
[21] K.S. Lee, W.S. Kim, T.H. Lee, A one-dimensional model for frost formation on a cold flat surface, Int. J. Heat Mass Transfer 40 (18) (1997) 4359–4365.
[22] M. Lee, Y. Kim, H. Lee, Y. Kim, Airside heat transfer characteristics of flat plate finned-tube heat exchangers with large fin pitches under frosting conditions, Int. J. Heat Mass Transfer 53 (2010) 2655–2661.
[23] M.-Y. Lee, Y. Kim, D.-Y. Lee, Experimental study on frost height of round plate fin-tube heat exchangers for mobile heat pumps, Energies 5 (2012) 3479–3491.
[24] R. LeGall, J.M. Grillot, Modeling of frost growth and densification, Int. J. Heat Mass Transfer 40 (13) (1997) 3177–3187.
[25] K. Lenic, A. Trp, B. Frankovic, Transient two-dimensional model of frost formation on a fin-and-tube heat exchanger, Int. J. Heat Mass Transfer 52 (2009) 22–32.
[26] P.J. Mago, S.A. Sherif, Frost formation and heat transfer on a cold surface in ice fog, Int. J. Refrig. 28 (2005) 538–546.
[27] M. Mahdavi, M. Yaghoubi, Experimental study of natural frost formation over a horizontal tube with annular compact fins under natural convection, Heat Transfer—Asian Res. 41 (2012) 84–98.

[28] B. Na, R.L. Webb, Mass transfer on and within a frost layer, Int. J. Heat Mass Transfer 47 (2004) 899–911.
[29] R.G. Rice, D.D. Do, Applied Mathematics and Modeling for Chemical Engineers, second ed., Wiley, N.J., 2012.
[30] C.N. Satterfield, T.K. Sherwood, The Role of Diffusion in Catalysis, Addison-Wesley, Reading, MA, 1963.
[31] Y.P. Su, Study of Thermofluid Characteristics of Plate and Louvered Finned-And-Tube Heat Exchangers under Frosting Conditions Master Thesis, Huafan University, Taipei, Taiwan, 2001.
[32] J. Villadsen, W.E. Stewart, Solution of boundary-value problems by orthogonal collocation, Chem. Eng. Sci. 22 (1967) 1483–1501.
[33] J. Villadsen, M.L. Michelsen, Solution of Differential Equation Models by Polynomial Approximation, Prentice-Hall, N.J., 1978.
[34] S. Whitaker, Simultaneous heat, mass, and momentum transfer in porous media: a theory of drying, in: J.P. Hartnett, T.F. Irvine (Eds.), Advances in Heat Transfer, vol. 13, Academic Press, NY, 1977, pp. 119–203.